

Multifunctional and Stimuli-Responsive Polydopamine Nanoparticle-Based Platform for Targeted Antimicrobial Applications

Nesha May O. Andoy,* Keuna Jeon, Christian Titus Kreis, and Ruby May A. Sullan*

The rising threat of antimicrobial resistance is a crisis of a global scale. If not addressed, it can lead to health care system problems worldwide. This warrants alternative therapeutic approaches whose mechanism of action starkly differs from conventional antibiotic-based therapies. Here, a multifunctional and stimuli-responsive (NIR laser-activated) antimicrobial platform is engineered by combining the intrinsic photothermal capability and excellent biocompatibility of polydopamine nanoparticles (PdNPs), with the membrane targeting and lytic activities of an antimicrobial peptide (AMP). The resulting PdNP-AMP nanosystem can specifically target and destabilize the mechanical integrity of the outer membrane of *Escherichia coli*, as measured using the atomic force microscope. Furthermore, the laser-induced nano-localized heating of PdNP—in close proximity to the already compromised bacterial envelope—induces further membrane damage. This results in a more efficient, laser-activated, bacterial killing action of PdNP-AMP. The antimicrobial platform developed in this work is shown to be effective against a drug-resistant *E. coli*. Overall, this work highlights the advantage and strength of combining multiple and coordinated biocidal mechanisms, into one nanomaterial-based system and its promise in treating drug-resistant pathogens.

1. Introduction

The rise of pathogens increasingly resistant to all known antibiotics is an alarming and pressing health care problem.^[1,2] Despite concerted global efforts in search of new antibiotics, with novel and more effective targets, bacteria will highly likely evolve to develop resistance.^[3] It is therefore imperative to *not* rely solely on “antibiotic-only-based therapies”, but to develop alternative therapeutic approaches, that is, different class of antimicrobials, whose mechanisms of action differ

from conventional antibiotics. These new class of antimicrobials should be effective against a broad spectrum of pathogens, and more importantly, should curb the emergence of further resistance.^[4,5]

One potential source of effective, bio-compatible, and broad-spectrum antimicrobials—whose targets are different from conventional antibiotics—are antimicrobial peptides (AMPs).^[6,7] AMPs are produced by all multicellular organisms as the first line of defense against invading pathogens.^[8] AMPs exhibit a variety of biocidal mechanisms: membrane lytic activity, enzyme inactivation, reactive oxygen species (ROS) induction, among others.^[9,10] However, not a single AMP bears all these desired functionalities. Furthermore, akin to antibiotics, it is also becoming apparent that bacteria can evolve resistance to AMPs.^[11] Nevertheless, due to their mechanism of action and pharmacodynamics, AMPs remain superior in preventing resistance evolution than conventional antibiotics.^[7,12] Hence,


similar to combinatorial antibiotic therapy, efficacious AMP cocktails have to be administered to achieve the synergistic effect ideal for combating multi-drug resistant organisms and limit resistance evolution.^[7]

Multifunctional antimicrobials, driven by nanotechnology, have recently emerged as another innovative solution to tackle microbial infections.^[5,13,14] As nanocarriers, nanomaterials can deliver a suite of antimicrobials to sites of infection.^[15] They can also exhibit intrinsic biocidal activities, enabling them to combine multiple and independent biocidal mechanisms into a single nanotherapeutic system.^[14] In particular, the ability of some nanomaterials to wreak physical damage to bacterial cells, via photothermal effects, is gaining interests owing to its killing mechanism different from conventional antibiotics.^[16–18] More importantly, the biocidal action of nanomaterials can be executed upon external stimulation. This means greater control in inducing bacterial inactivation—potentially delaying the onset of resistance evolution.^[14,17] Several nanomaterials have already been used for photothermal inactivation of bacteria.^[19] Among these, gold nanoparticles have been the most extensively studied.^[19–22] With its excellent photothermal conversion efficiency and facile surface functionalization, gold nanoparticles are popular multifunctional antibacterial photothermal

Dr. N. M. O. Andoy, K. Jeon, Dr. C. T. Kreis, Prof. R. M. A. Sullan
Department of Physical and Environmental Sciences
University of Toronto Scarborough
1065 Military Trail, Toronto, ON M1C 1A4, Canada
E-mail: nesha.andoy@utoronto.ca; ruby.sullan@utoronto.ca

K. Jeon, Prof. R. M. A. Sullan
Department of Chemistry
University of Toronto

80 St. George St., Toronto, ON M5S 3H6, Canada

 The ORCID identification number(s) for the author(s) of this article can be found under <https://doi.org/10.1002/adfm.202004503>.

DOI: 10.1002/adfm.202004503

agents.^[18,23,24] Notwithstanding, in vivo applications of gold nanomaterials remain limited due to their cytotoxic effects.^[25,26] Thus, the search for alternative photoactive nanomaterials that are highly biocompatible continues to be an ongoing effort.

Polydopamine nanoparticle (PdNP) is a bio-inspired nanomaterial that has been shown to be an effective photothermal agent against tumor cells, both in culture and in animal models.^[27] Consisting only of polymerized dopamine, a neurotransmitter already found in the body, cells treated with PdNP are not subjected to the toxic effects of foreign substances. Experiments done on rats demonstrate that PdNP is biodegradable and does not induce any acute or long-term toxicity effects.^[27] Furthermore, the facile nature of PDNPs toward surface bioconjugation, also makes them highly tunable for specific bacterial targeting, a crucial pre-requisite toward precision therapeutics.^[28]

Though polydopamine-based nanoparticles have been thoroughly studied as anti-cancer photothermal agents,^[29] their utility toward antimicrobial applications has not been extensively explored. Rather, polydopamine has mostly been used as coatings for rendering surfaces with antimicrobial properties, or as photothermally active biocidal film to prevent fouling.^[30–33] As it is easier to thermally kill mammalian cells than bacteria, localized photothermal heating (i.e., focused on areas in close proximity to the pathogen surface) is required for in vivo applications, to avoid damaging the surrounding mammalian cells.^[16,34] An effective strategy involves modifying the surface of PdNP with bacterial targeting molecules.^[35,36] This brings the nanoparticles very close to the bacterial membrane, transforming them into “localized nano-heaters” upon laser irradiation.^[35] This strategy has also been extensively used in other photothermally active nanomaterials.^[20,21,37] Photothermal treatment (PT) in this case will then only require lower energy input to kill both Gram-positive and Gram-negative bacteria.^[35,36]

In this work, we show that beyond acting as localized nano-heaters, PdNPs can be further engineered with an additional biocidal mechanism highly complementary to its photothermal activity—resulting in a more effective antimicrobial agent. We combine 1) the photothermal capability and biocompatibility of PdNP with 2) AMP’s bacterial membrane targeting and lytic activities to engineer a multifunctional antimicrobial that targets and kills bacteria via multiple and coordinated biocidal mechanisms. By decorating the surface of PdNP with a membrane-active peptide, we show that the cooperative effects between the peptide’s membrane-destabilizing activity and PdNP’s laser-induced heating capability can drastically lower the mechanical stability of *Escherichia coli*’s outer membrane. This in turn led to a significant drop in the critical solution temperature needed for *E. coli* cell death upon laser irradiation. Furthermore, we show that the combination of these multiple biocidal mechanisms—different from conventional antibiotics—is effective against an antibiotic resistant *E. coli*.

2. Results and Discussion

2.1. Synthesis and Characterization of PdNPs

PdNPs were synthesized via oxidative polymerization of dopamine by saturated O₂ in 10 mM Tris buffer pH 11 (Figure 1a inset). The growth of PdNP was monitored using dynamic light scattering (DLS). Within 1 h of reaction, particles with hydrodynamic size of ≈45 nm already started to appear and gradually increased in diameter (D_h) over time (Figure 1a). The surface charge of the nanoparticles harvested after 24 h was characterized using phase analysis light scattering (PALS). At pH 7.5, PdNP bears a zeta potential of -33 ± 3 mV (Figure 1b), consistent with what has been reported for both polydopamine particles and films.^[38,39]

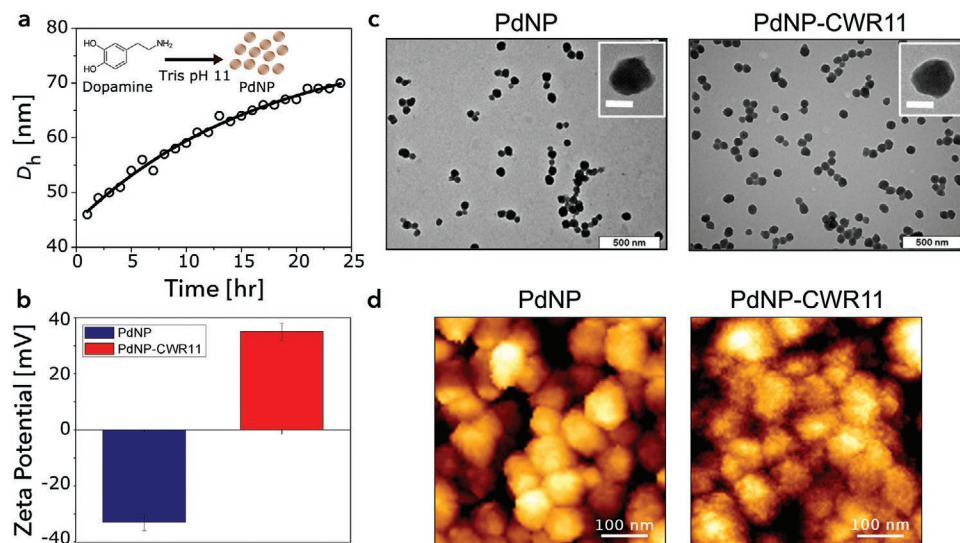


Figure 1. PdNP synthesis, functionalization, and characterization. a) Growth kinetics of PdNP, measured by DLS, showing the gradual increase of the hydrodynamic diameter (D_h) with time (solid line is an exponential fit). Inset: Schematic of PdNP formation via autooxidation of dopamine in Tris buffer pH 11. b) Surface zeta potential (at pH 7.5), c) TEM images, and d) AFM topography images in buffer, of PdNP before (left) and after (right) functionalization with the antimicrobial peptide, CWR11 (PdNP-CWR11). Inset in (c): Higher magnification image, scale bar = 50 nm.

To determine the size and shape of the synthesized PdNP, we visualized the nanoparticles via transmission electron microscopy (TEM) and atomic force microscopy (AFM) imaging. The representative TEM image in Figure 1c shows that the nanoparticles are generally spherical in shape, with mean diameter of 85 ± 18 nm (Figure S1a, Supporting Information). The shape and size are confirmed with AFM imaging, where an average nanoparticle diameter of $\approx 87 \pm 13$ nm was determined from topography images obtained in liquid environment (Figure 1d; Figure S1b, Supporting Information). Spectroscopic measurements on PdNP further confirmed its formation (Section S1, Supporting Information): i) optical absorption spectroscopy (Figure S2a, Supporting Information), showing the characteristic broad absorption spectrum of PdNP solutions from UV to near-infrared (NIR) regions and ii) Fourier-transform infrared (FTIR) spectroscopy (Figure S2b, Supporting Information), which shows the characteristic peaks for polydopamine.

2.2. Surface Modification of PdNP with the Antimicrobial Peptide, CWR11

The intrinsic chemical reactivity of polydopamine-based materials makes PdNP readily tunable for different surface modifications. In particular, the presence of catechol renders them highly reactive toward thiol-containing compounds via Michael addition.^[28] Leveraging on this facile surface functionalization, we modified the surface of PdNP with an antimicrobial peptide, CWR11 (CWFWKWRRRRR), via a cysteine residue on its N-terminus. CWR11 is an engineered arginine-tryptophan-rich peptide, potent against a broad spectrum of bacteria.^[40] By mixing CWR11 with PdNP in buffer at pH 8.5, the surface of the nanoparticle was decorated with CWR11 (see Section S1, Supporting Information). Figure 1b shows that the zeta potential of PdNP after CWR11 functionalization (PdNP-CWR11) shifted to positive values, 35 ± 3 mV (vs -33 mV for bare PdNP). Since CWR11 has a net +6 charge at pH 7.5, surface modification with CWR11 is expected to shift the surface potential from negative (bare PdNP) to positive (PdNP-CWR11). Successful grafting of CWR11 onto PdNP was further confirmed with optical absorption and FTIR spectroscopies in Figures S2a and S2b, respectively, Supporting Information. In addition, the PdNP was imaged using TEM after surface functionalization with CWR11 (Figure 1c). No significant changes were observed on both the size $\approx 84 \pm 17$ nm (vs 85 ± 18 nm for bare PdNP; Figure S1a, Supporting Information) and surface features of the nanoparticles (Figure 1c insets). This is consistent with a prior study where TEM imaging is not able to resolve surface modification of polydopamine nanoparticles with PEG polymers.^[41] Unlike TEM, however, AFM imaging in liquid can differentiate between CWR11-modified PdNP from bare particles. Figure 1d shows that in PdNP-CWR11, nanometer scale “protrusions” uniformly decorate the surface of the nanoparticle. This slightly increased the measured diameter of PdNP-CWR11 to $\approx 92 \pm 14$ nm (vs 87 ± 14 nm (red) in Figure S1b, Supporting Information). The ability of AFM to obtain high-resolution structural information, in liquid environment and under ambient conditions, provides us with a nanoscale picture of what the bacteria will encounter when in contact with the bare

nanoparticle and when the nanoparticle is decorated with the antimicrobial peptide in solution. This highlights the utility of nanoscale imaging under physiological conditions, in the characterization of nanomaterials for biological applications.

2.3. Photothermal Capability of PdNP and Its Killing Action Toward *E. coli*

The broad absorption spectrum of PdNP that extends all the way to the NIR region (Figure S2a, Supporting Information), along with its excellent biocompatibility, makes it an ideal photothermal (PT) agent for in vivo applications.^[27,42] With PdNP, the optical excitation can be tuned to energies within the “biological window” or “NIR window” (i.e., 670–890 nm)—the spectral region for optimal tissue penetration with minimal (non-selective) heating.^[34] PdNP has already been proven effective as PT agent against cultured tumor cells and in tumor-bearing mouse model.^[27] In the current work, we show that PdNP’s ability for laser-induced photothermal heating can also be utilized to effectively disable planktonic *E. coli* cells. Using a continuous wave (CW) 0.4 W 808 nm laser (diameter ≈ 3 mm), we first measured the PdNP-induced photothermal heating of aqueous solutions. Figure 2a monitors the change in solution temperature as a function of PdNP concentrations during continuous laser irradiation, as measured using a thermal imager (Figure S4a, Supporting Information). It is clear that the temperature change is dependent on PdNP concentration; while no significant increase was observed in pure water (Figure 2a, black), temperatures close to 50 °C (from RT = 22 °C) were observed in the presence of 1 nM PdNP (Figure 2a, cyan). Figure 2a also shows that the maximum temperature was reached after only a few minutes of laser illumination and remained stable for the whole duration of laser exposure (i.e., 20 min).

Next, we tested the efficiency of laser-induced photothermal heating of PdNP toward bacterial cell death of a drug-resistant strain of *E. coli* AR3110, a cellulose producing K12 *E. coli* that readily forms biofilms.^[43] Using spread plate assay, we quantified the effect of photothermal heating on bacterial growth (Figure S4c, Supporting Information). The number of viable *E. coli* cells decreases in a sigmoidal manner with increasing PdNP concentrations (Figure 2b). Fitting the data with a modified Gompertz (mGompertz) function^[44] (Figure 2b, solid line), we determined the minimal inhibitory concentration (MIC) to be 1.0 ± 0.1 nM PdNP, for the 20 min photothermal treatment of *E. coli*. We can infer from Figure 2a that at 1 nM PdNP, solution temperature can go up to >48 °C (also see Figure S4a, Supporting Information). This implies that under our experimental condition, the thermally induced cell death of *E. coli* occurs at temperatures close to 48 °C. This is in agreement with previous works, which show that growth rate of *E. coli*, as well as other mesophilic Gram-positive and Gram-negative bacteria, precipitously drops at a critical temperature (T_c) of ≈ 47 °C.^[45,46] A cell-wide structural proteomic analysis had shown that at T_c , cell death is driven by the thermal denaturation and loss of function of a subset of essential proteins, which for *E. coli* peaks precisely at 47 °C.^[46] With laser-induced photothermal heating, PdNP solutions (as low as 1 nM) can readily reach this critical temperature. This strongly demonstrates that the laser-induced

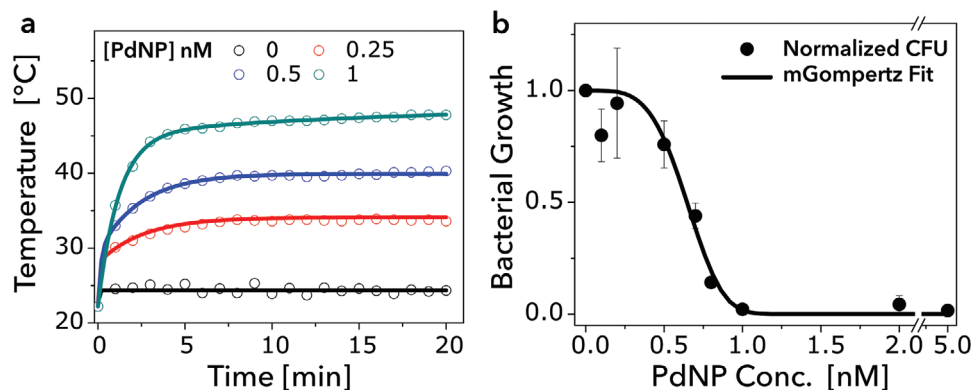


Figure 2. PdNP as a photothermal agent. a) Continuous laser irradiation (CW 808 nm, 0.4 W, diameter = 3 mm) of aqueous solutions of PdNP increases the temperature of the solution in a concentration-dependent manner (solid lines are exponential fits). b) Normalized bacterial growth of *E. coli* after 20 min laser irradiation at different PdNP concentrations. Data was fitted with Lambert and Pearson's modified Gompertz model: MIC = 1.0 ± 0.1 nM and NIC = 0.46 ± 0.05 nM. MIC, minimum inhibitory concentration; NIC, non-inhibitory concentration.

photothermal heating of PdNP is an effective strategy that can be used to kill bacteria in a stimuli-responsive, that is, laser-activated manner.

A huge challenge however, in the in vivo killing of pathogens using optically heated nanomaterials, is minimizing collateral damage to surrounding healthy cells while specifically targeting the bacteria. It only requires temperatures upward of 42 °C to kill human cells, while ≥ 47 °C is needed to thermally destroy most mesophilic pathogens.^[45] In addition, due to the high surface area-to-volume ratio of microorganisms, higher particle and laser power densities are required to achieve hyperthermia-induced bacterial cell death.^[16] Our attempt to mitigate these challenges is to decorate the surface of PdNP with antimicrobial peptides (AMP), which are generally selective toward targeting bacterial cell membranes over host mammalian cells.^[10]

2.4. Biocidal Activity of the Antimicrobial Peptide, CWR11

The antimicrobial peptide used in our work, CWR11, has been shown to be an effective antimicrobial against a broad spectrum of pathogens—both Gram-negative and Gram-positive bacteria.^[40] Lim et. al. engineered CWR11 to have both bacterial membrane targeting and destabilizing actions.^[40] They have also shown that CWR11 retains its antimicrobial activity even after surface immobilization. This makes CWR11 an ideal proof-of-principle peptide to test the effectivity of AMP-decorated PdNP as a multifunctional nanomaterial-based antimicrobial. As such, we tested whether CWR11 is active against the tetracycline resistant (Tet-resistant) strain of *E. coli* (AR3110), as it was against a non-drug resistant strain (ATCC 8739).^[40] Using spread plate assay in the presence of increasing peptide concentrations, we show that CWR11 can also inactivate *E. coli* AR3110, with MIC = 3.8 ± 0.2 μ M, in the presence of 100 mM NaCl (Figure 3a; Figure S5a, Supporting Information). We note that like most AMPs, CWR11 has a higher killing efficiency at lower salt concentrations (Figure S5b,c, Supporting Information). Overall, our results align with what was previously reported for CWR11 against the non-drug resistant strain of *E. coli*. We highlight that due to the differences in the antimicrobial actions

between CWR11 and tetracycline, CWR11 remained effective in killing the Tet-resistant strain of *E. coli*. The wide variety of AMP's cellular targets, and biocidal mechanisms different from most antibiotics, render AMPs as viable alternatives to antibiotics, especially in tackling antibiotic-resistant pathogens.^[12]

2.5. Mechanism of Antimicrobial Action of Free CWR11

As mentioned, CWR11 was engineered to have a membrane destabilizing activity. Prior SEM images of CWR11's lytic action on *E. coli* resulted in corrugation of the outer membrane.^[40] This phenomenon is commonly observed when *E. coli* is treated with other membrane-destabilizing AMPs.^[47,48] Contrary to the well-accepted paradigm on the role of cell wall in imparting stability to the bacterial cell envelope, a recent study has shown that the outer membrane is a major contributor to *E. coli*'s mechanical integrity.^[49] We hypothesized that AMP-induced structural damage could also alter the outer membrane's mechanical property. To investigate further the membrane-destabilizing activity of CWR11 against *E. coli* AR3110, we simultaneously monitored the structural and mechanical properties of *E. coli* cells, before and after treatment with CWR11, using AFM Quantitative Imaging (QI).^[50,51] With QI, we can directly correlate changes in the membrane's structure with changes in its mechanical properties (elasticity). Furthermore, as measurements are done under physiological conditions, we can monitor the action of CWR11 on *E. coli* membrane in situ—eliminating the need for sample fixation and drying—thus giving a more physiological picture of the state of bacteria upon exposure to a membrane active AMP.^[47]

Representative AFM images of *E. coli* before and after CWR11 treatment are shown in Figure 3b. AFM images show that while *E. coli* (control) has a relatively smooth surface, the outer membrane of the bacteria, when exposed to MIC concentrations of CWR11, exhibits wrinkling/corrugation (Figure S6, Supporting Information, for more examples). While the topography images clearly show the effect of CWR11 on the structure of the outer membrane (Figure 3b), the corresponding Young's modulus map for each bacterium quantify the accompanying changes in

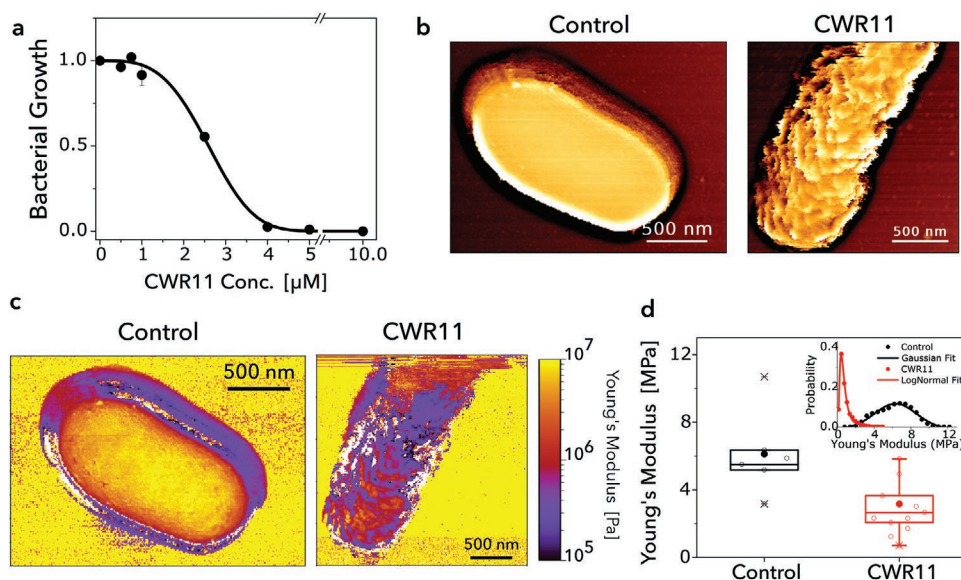


Figure 3. Biocidal action of CWR11 on *E. coli*. a) Normalized bacterial growth with increasing CWR11 concentrations; data fitted with modified Gompertz function: MIC = $3.8 \pm 0.2 \mu\text{M}$ and NIC = $1.8 \pm 0.1 \mu\text{M}$. b) AFM topography images and c) corresponding Young's modulus (elasticity) maps before (left) and after (right) treatment with $4 \mu\text{M}$ CWR11, respectively. d) Box plots of elasticity values from many individual bacteria: before (control, black, $n = 6$) and after (CWR11, red, $n = 13$) treatment with CWR11. Inset: Histogram of elasticity values obtained from each bacterium in (c). Fits shown are from Gaussian (black) and log-normal distribution (red).

the elasticity (E) of the cell envelope upon peptide treatment. The Young's modulus is a mechanical property that measures stiffness of materials, thus, the response of *E. coli* to applied forces. As such, it can be used as a metric for the bacterial envelope's mechanical stability/integrity. Figure 3c (left) shows that the structurally smooth surface features of *E. coli* correspond to a homogeneously distributed elasticity values: $E_{\text{control}} = 6 \pm 3 \text{ MPa}$ (Figure 3D, inset, black; also see Section 4 in Supporting Information)]. Meanwhile, the corrugated membrane morphology (i.e., the ruffled structure) observed for CWR11-treated *E. coli* correlates with lower elasticity values (purple) in the Young's modulus map (Figure 3c, right). This demonstrates that upon peptide treatment, the average bacterial stiffness is drastically decreased: $E_{\text{CWR11}} = 0.7 \pm 0.4 \text{ MPa}$ (Figure 3d, inset, red). Combining all average elasticity values from many individual bacteria, Figure 3d shows that CWR11 treatment renders the elasticity of the outer envelope less resistant (i.e., softer bacterial envelope) to the applied nano-indentation forces than without AMP treatment: $E_{\text{CWR11}} = 3 \pm 2 \text{ MPa}$ ($n = 14$) versus $E_{\text{control}} = 6 \pm 2 \text{ MPa}$ ($n = 6$). These correlated structural and stiffness measurements show that CWR11 does not only alter membrane morphology, but also causes membrane destabilization, enough to lower the ability of *E. coli*'s bacterial envelope to resist small forces (1 nN maximum). As the outer membrane of Gram-negative bacteria plays a pivotal role in its mechanical stability and its ability to screen some antibiotics, CWR11's ability to alter the structure and weaken the mechanical integrity of this protective layer highlights its potential to contribute significantly to the antimicrobial activity of CWR11-decorated PDNP.

The membrane destabilizing/lytic ability of CWR11 was also confirmed with fluorescence microscopy using SYTO9 and propidium iodide (PI) probes. SYTO9 can penetrate intact membranes, hence can make all cells (live or dead) fluoresce

green; PI can only penetrate cells with damaged membranes, so only cells with compromised membranes will fluoresce red. Figure 4a,b shows fluorescence images of *E. coli* cells before and after treatment with CWR11 (at MIC = $4 \mu\text{M}$), respectively. Without CWR11 (Control), *E. coli*'s outer and cytoplasmic membranes are intact, making them only permeable to SYTO9—resulting in green fluorescent cells with almost no red cells. Areas enclosed in white squares—magnified, rightmost panels—highlight that for bacteria labeled with PI, the fluorescence coming from SYTO9 is quenched (white arrows). After treatment with CWR11 (Figure 4b), most of the cells were stained with the red fluorescent PI, while also quenching the fluorescence of SYTO9 (magnified panels, white arrows), similar to the control. This further demonstrates that CWR11 can disrupt and destabilize both the outer and cytoplasmic membranes of the Tet-resistant *E. coli* AR3110, similar to what was observed for *E. coli* ATCC 8739.^[40]

2.6. PdNP-CWR11's Antimicrobial Activity and Mechanism of Action

With the membrane destabilizing effects of CWR11 on a drug resistant *E. coli* confirmed, the effects of surface immobilization on the antimicrobial activity of CWR11 was measured next. The viability of *E. coli* as a function of increasing PdNP-CWR11 concentrations (without laser treatment) was monitored (Figure 5a, green). After 20 minutes of incubation with PdNP-CWR11, the number of viable bacteria decreased with increasing PdNP-CWR11 concentrations, with MIC = $1.9 \pm 0.3 \text{ nM}$. As PdNP alone does not exhibit any antimicrobial activity (Figure S8A, Supporting Information), our growth assay confirms that the antimicrobial activity of CWR11 bound to PdNP is retained. The ability of PdNP-bound CWR11 to induce membrane

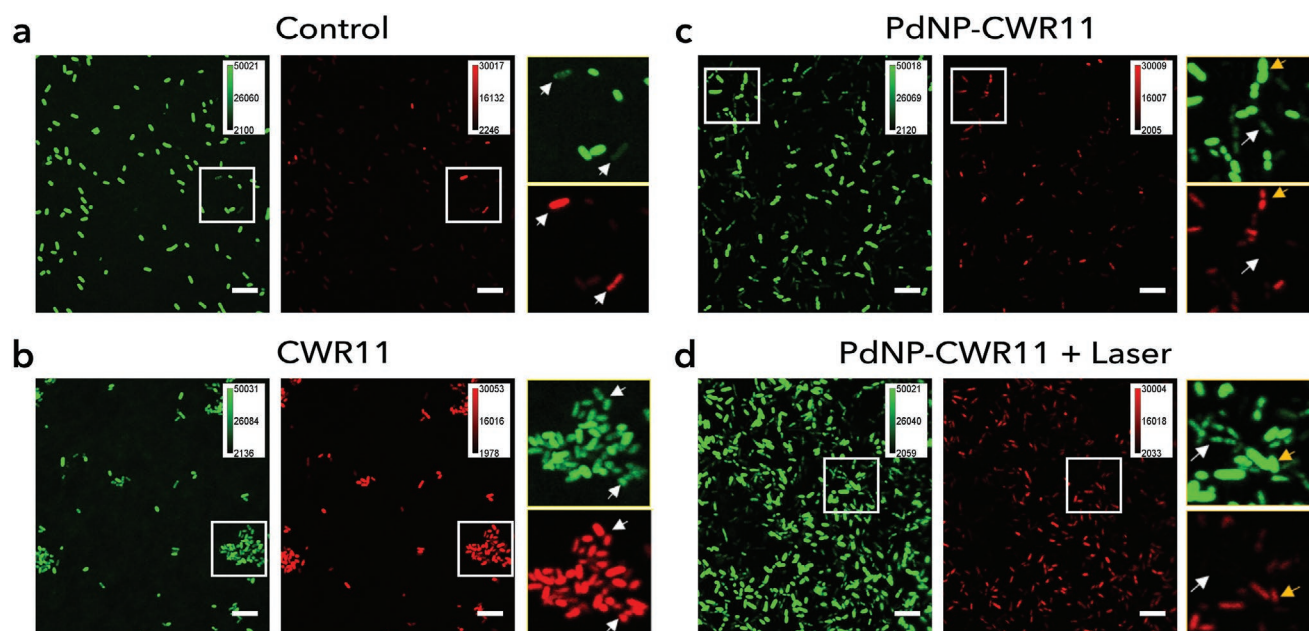


Figure 4. Fluorescence microscopy of a) control *E. coli* in buffer, and in the presence of b) free antimicrobial peptide, CWR11, c) CWR11 bound to PdNP, and d) PdNP-CWR11 with laser irradiation. Shown are bacteria stained with SYTO9 (green channel) and propidium iodide, PI (red channel) of the same area. Areas highlighted within the white squares are magnified on the rightmost column: i) white arrows on both green and red channels highlight bacteria with quenched SYTO9 fluorescence and ii) orange arrows highlight PI-stained bacteria without quenched SYTO9 fluorescence.

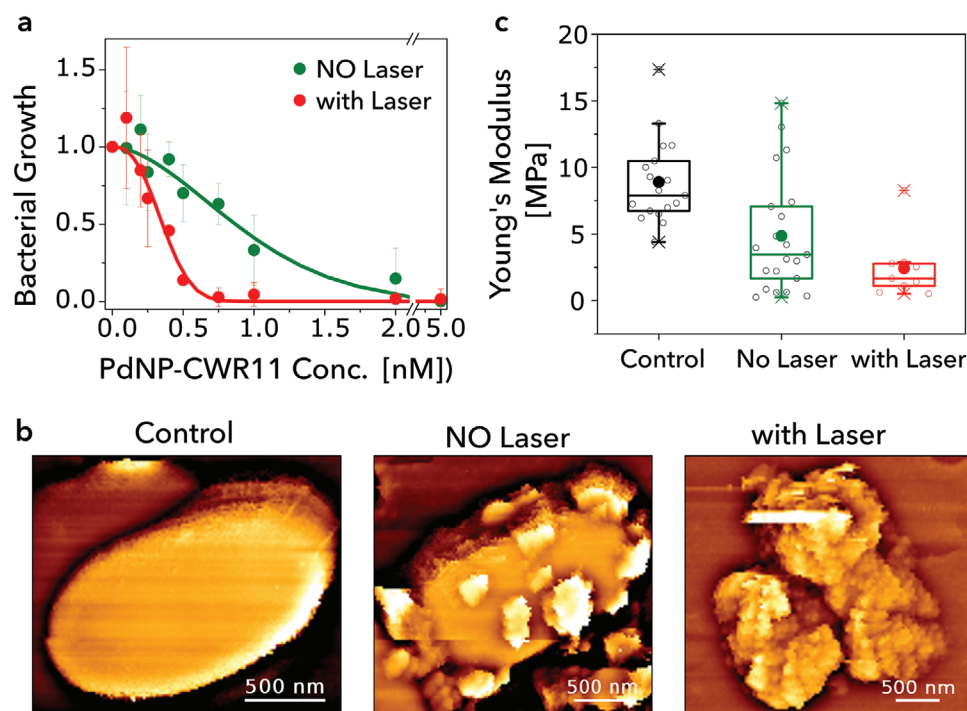


Figure 5. PdNP-CWR11 as a multifunctional antimicrobial agent. a) *E. coli*'s normalized bacterial growth in the presence of increasing PdNP-CWR11 concentrations, without (green) and with (red) laser irradiation. b) AFM topography images of *E. coli* in M9 media (leftmost panel) and in the presence of PdNP-CWR11 (middle panel). Rightmost panel shows *E. coli* in the presence of PdNP-CWR11 after 20 min laser irradiation, showing more physical damage than without laser treatment. c) Distribution of the average Young's modulus from many individual bacteria. The elasticity of *E. coli* in M9 media ($E_{\text{control}} = 9 \pm 3$ MPa, black, $n = 18$) is higher than in PdNP-CWR11 decorated *E. coli* ($E_{\text{NO Laser}} = 5 \pm 4$ MPa, green, $n = 21$). *E. coli* mixed with PdNP-CWR11 and further treated with laser has the lowest average elasticity value ($E_{\text{with Laser}} = 2 \pm 2$ MPa, red, $n = 9$).

destabilization and/or cell death was further confirmed with fluorescence microscopy. Compared to the control (Figure 4a), the number of *E. coli* stained with PI increases when cells are incubated with PdNP-CWR11 (Figure 4c). Unlike the free CWR11 (Figure 4b), however, the intensity of PI staining is decreased. For those that did stain with PI, SYTO9 fluorescence was not quenched (Figure 4c, magnified panels, orange arrows). We also observed several bacteria with quenched SYTO9 fluorescence but with no PI staining (Figure 4c, magnified panels, white arrows). We take this as due to fluorescence quenching in the presence of PdNP, which has previously been shown to quench the fluorescence of different dyes via FRET and/or direct electron transfer.^[52]

Both the increase in PI staining (vs control) and the antimicrobial activity (Figure 5a, green) of PdNP-CWR11 provide evidence that surface-bound CWR11 still retained its membrane destabilizing/biocidal activity, albeit not as efficient as the unbound or free CWR11. Based on the density of CWR11 molecules that bind to the surface of PdNP (see Section S1, Supporting Information, for details), we estimate that the antimicrobial activity of immobilized CWR11 is $\approx 10\times$ lower compared to free CWR11. This is in line with prior works, which reported loss of activity of AMPs upon surface immobilization, with some reducing their activity as much as 100-fold.^[53,54] We posit that in our system, one major contributor for the loss in antimicrobial activity of CWR11 is the physical constraint imposed by the binding of the nanoparticle to the surface of *E. coli*—only a fraction of the PdNP-CWR11 surface can interact with *E. coli* at a time, therefore reducing the “number of CWR11” available for bactericidal action (Figure 5b, middle panel). Also, since the presence of linkers has been shown to influence the activity of surface immobilized AMPs,^[54,55] we are currently exploring how different linker lengths (PEG-linker) improve the activity of surface-bound AMP.

In addition to CWR11's antimicrobial activity, one key advantage in decorating the surface of the polydopamine nanoparticle with the peptide is facilitated targeting and binding to bacterial membranes. We show in Figure 5b (middle panel) that the surface of *E. coli* can indeed be decorated with clusters of PdNP-CWR11. This is in huge contrast to images obtained for *E. coli* in the presence of just the bare PdNPs, where nanoparticles were mostly found on the substrate and not bound to the bacteria (see white circles in Figure S9A, Supporting Information). Here, the topography images of the bacterial surface are devoid of prominent features. With PdNP-CWR11, on the other hand, we found that most of the nanoparticles were bound to the surface of *E. coli*, with barely any on the substrate (Figure S9b, Supporting Information). This strongly points to the more efficient binding of PdNP-CWR11 to bacterial membranes compared to bare PdNP. The non-binding of bare PdNP could be attributed to the electrostatic repulsion between the negatively charged PdNP surface (Figure 1b) and the anionic character of the outer membrane of Gram-negative bacteria, due to the presence of lipopolysaccharide and negatively charged lipid molecules.^[56] The surface of PdNP-CWR11, on the other hand, is decorated with CWR11, which has five positively charged arginine (R) residues for electrostatic interactions with bacterial membranes and 4 tryptophan (W) residues for membrane insertion. This makes PdNP-CWR11, by design, able to target and interact with the surface of *E. coli* membrane much stronger than bare PdNP.

The surface immobilization of CWR11 did not only enhance the antimicrobial activity of PdNP but also led to a significant reduction in AMP's hemolytic activity—one of the main hurdles for the successful clinical application of AMPs.^[12] Figure S11, Supporting Information, shows that CWR11, being positively charged and highly hydrophobic, is a highly hemolytic AMP, with $\approx 40\%$ activity at its MIC ($4\ \mu\text{M}$). After immobilization on the surface of PdNP, the hemolytic activity of PdNP-CWR11, at the MIC of PdNP-CWR11 + laser (1 nM), was dramatically reduced to $\approx 2\%$, a $20\times$ reduction. This strongly demonstrates that the combination of different antimicrobial mechanisms into one nanosystem could not only increase the antimicrobial activity but also mitigate their limitations (i.e., toxicity).

2.7. Effect of PdNP-CWR11 on the Mechanical Stability of the Outer Envelope

Despite having a preferential binding affinity toward *E. coli*'s outer membrane, PdNP-CWR11 did not induce membrane ruffling as what was observed with free CWR11 (Figure 5b middle panel vs Figure 3b right panel). We therefore measured whether PdNP-CWR11 binding can still change the mechanical stability of the outer membrane. The average elasticity or Young's modulus values (Figure 5c) for many individual bacteria before (black, $n = 18$) and after (green, $n = 21$) treatment with PdNP-CWR11 clearly demonstrates that, similar to free CWR11, binding of PdNP-CWR11 to *E. coli* also lowered bacterial stiffness, from 9 ± 3 MPa (control) to 5 ± 4 MPa (Figure S10, Supporting Information). Since PdNP alone does not change the stiffness of *E. coli* (Figure S8b, Supporting Information), our results indicate that despite the lack of membrane ruffling, CWR11 bound to PdNP still destabilizes the membrane. Our data further suggests that partial membrane coverage of PdNP-CWR11 is enough to induce membrane destabilization and cell death. We note that a correlation between PdNP-CWR11 surface coverage and how it changes bacterial stiffness cannot (yet) be established under our current experimental condition—the AFM tip cannot access the other side of *E. coli* (i.e., side facing the substrate), making surface coverage measurements not possible. Quantifying surface coverage and its correlation to changes in bacterial elasticity is an ongoing effort in the lab. Despite this present limitation, our correlated imaging of the bacteria's mechanical properties and surface structures has shown that decorating PdNP with CWR11 clearly augments the nanoparticle's bacterial targeting and deactivating capabilities. Furthermore, AFM imaging has shown that PdNP-CWR11 binds the surface of *E. coli* in clusters. This will have important implications in PdNP-CWR11's effectiveness as a photothermal agent, as hyperthermia is more efficient for clusters of, rather than individual, photoactivable nanoparticles.^[16,21,57]

2.8. Synergistic Effect of PTT and CWR11 on the Antimicrobial Activity of PdNP-CWR11

The ability of PdNP to kill *E. coli* via laser-induced photothermal heating and CWR11's membrane destabilizing activity makes PdNP-CWR11 a multifunctional antimicrobial nanotherapeutic

system, i.e., having two different mechanisms to kill pathogenic microorganisms. We therefore tested the effect of having both biocidal mechanisms to the ability of PdNP-CWR11 to inactivate *E. coli* after laser treatment. Figure 5a (red) shows that laser irradiation of PdNP-CWR11 solutions kills *E. coli* more effectively than without the laser-induced photothermal heating, with MIC = 0.6 ± 0.1 nM (vs 1.9 ± 0.3 nM; Figure 5a, green). Fluorescence imaging further confirms that with the same PdNP-CWR11 concentration (1 nM), laser illumination caused the number of cells stained with PI (as well the intensity of PI staining) to increase (Figure 4d). When compared with bare PdNP (Figure S12, Supporting Information, replotted for direct comparison), PdNP-CWR11 further showed improved effectivity as a photothermal agent, with MIC improving by almost twofold. While these improvements in MIC may not seem significant at first look, we highlight that laser irradiation in the presence of PdNP-CWR11 was able to kill *E. coli* at a much lower temperature. From Figure 2a, we can estimate that the maximum temperature reached during laser illumination of 0.6 nM PdNP is <47 °C, and should only be slightly above 40 °C (for 0.5 nM PdNP). We can extrapolate that with PdNP-CWR11, the critical temperature needed to kill *E. coli* is much lower than what is expected for the thermally induced cell death of *E. coli*. This implies that the mechanism of bactericidal action of PdNP-CWR11 is different from general hyperthermia—where solution temperature of at least 47 °C is necessary to kill the bacteria. Our experimental data suggests that with PdNP-CWR11, the laser-induced *E. coli* cell death is triggered by “localized pasteurization,” where clusters of nanoparticles bound to the surface of *E. coli* enables heat transfer directly to the bacterial envelope leading to more structural damage.^[16] AFM topography images of PdNP-CWR11-treated *E. coli* after laser treatment supports this scenario (Figure 5b, right most panel; see Figure S9c, Supporting Information, for more examples). The significant photothermal-induced structural damage also leads to much lower Young’s modulus, $E = 2.4 \pm 2.3$ MPa (Figure 5c, red).

CWR11 also affects the minimum concentration at which we start to observe photothermally induced bacterial growth impairment, that is, non-inhibitory concentration (NIC). With laser irradiation, bacterial growth starts to decrease at [PdNP-CWR11] > 0.2 nM ($\text{NIC}_{\text{PdNP-CWR11}} = 0.21 \pm 0.04$ nM), while for bare PdNP, $\text{NIC}_{\text{PdNP}} = 0.46 \pm 0.05$ nM (Figure 2b; Figure S11, Supporting Information). This implies that with laser treatment, at nanoparticle concentrations between ≈ 0.2 and ≈ 0.46 nM, while we generally see no effect on bacterial viability for bare PdNP, we expect to see bacterial growth inhibition with PdNP-CWR11. All these suggest that the presence of CWR11 on the surface of PdNP did not merely add another bactericidal action to the nanoparticle, rather the cooperative effects between CWR11’s antimicrobial activities and PdNP’s photothermal ability enabled a more efficient bacterial killing activity. Since PdNP-CWR11 binding can already destabilize the outer membrane of the bacteria, additional laser-treatment to the already-compromised bacterial envelope could facilitate a more efficient “localized pasteurization” for bacterial inactivation, reducing the amount of nanoparticle needed to thermally induce cell death in *E. coli*. This will have implications on how PdNP-CWR11 could potentially reduce collateral damage to healthy tissues surrounding

bacterial infections, as general hyperthermia (i.e., $T \geq 47$ °C) is no longer necessary to inactivate the pathogens.

These results are consistent with prior works, which show that the bacterial surface targeting activity of Magainin I and vancomycin enabled PdNP to localize heating closer to the bacteria, leading to a significant lowering of temperature required for the photothermal killing of pathogens.^[35,36] Together with these studies, our work showcases the general applicability of PdNP-based nano-system as a viable alternative for in vivo photothermal antimicrobial applications. By decorating the surface of PdNP with a membrane-active peptide, we have shown that the peptide’s membrane-destabilizing activity greatly enhanced the effect of PdNP’s laser-induced heating capability in lowering the mechanical stability of *E. coli*’s outer membrane. This led to a significant drop in the critical solution temperature needed to kill *E. coli*, making CWR11-modified PdNP more effective as a photothermal antimicrobial agent. Furthermore, PdNPs have also been used as nanocarriers for small molecule antimicrobial to kill bacteria via other mechanisms (e.g., antibiotics, ROS-, and NO-induced bactericidal activities) or to augment its photothermal capability in killing microorganisms.^[58–61] This makes PdNP an overall versatile nanomaterial-based antimicrobial agent, highly tunable and capable of delivering multiple biocidal mechanisms drastically different from conventional antibiotic-only based therapies.

3. Conclusion

Overall, our results demonstrate that the combined membrane targeting and destabilization activities of CWR11 and the localized photothermal-heating of PdNP could result in a multifunctional and stimulus-responsive (laser-induced) antimicrobial. This multi-functionality makes PdNP-CWR11 not just capable of killing bacteria, but also enables it to potentially mitigate collateral damage to healthy cells surrounding sites of infection by lowering the critical temperature needed to inactivate bacteria. This strongly points to the utility of combining different, yet complementary biocidal mechanisms, into one nano-system. Their cooperative effects can create a new class of antimicrobial whose mechanism of action can be tuned to be effective in treating antibiotic resistant organisms. Furthermore, due to the stimuli-responsive activity of PdNP-CWR11 (laser-induced heating), its bactericidal activity can also be deployed in a more targeted and controlled manner, potentially reducing the probability of resistance evolution.

4. Experimental Section

Materials: Dopamine (3,4-dihydroxyphenylalanine) hydrochloride was purchased from Fisher Scientific (Canada). Tris hydrochloride, bicine, sodium chloride, sodium hydroxide, potassium chloride, poly(ethylenimine) (PEI), and tris(2-carboxyethyl)phosphine (TCEP) were from Sigma-Aldrich (Canada). The CWR11 peptide was purchased from GenScript USA Inc. *E. coli* AR3110 strain, with tetracycline resistance (pMP7604), used in the current work was a gift from Regine Hengge’s laboratory of Institut für Biologie/Mikrobiologie, Humboldt-Universität zu Berlin. Live/dead BacLight Viability Kit (Invitrogen, kit L7012) was used for PI/SYTO9 staining. Buffers used: Tris buffer pH 11 (10 mM) and 10 mM Bicine buffer pH 8.5 with 100 mM NaCl and 2.7 mM KCl (BBS).

Nanoparticle Synthesis: PdNPs can be formed via the autoxidation of dopamine in alkaline solution. In this work, PdNP was synthesized using 0.6 mg mL⁻¹ solution of dopamine hydrochloride in Tris buffer pH 11 (10 mM) with constant shaking (60 rpm) for 24 h in the dark at RT. The formed nanoparticles were purified by centrifugation at 15 000 g for 30 min and washed 3× with ultrapure water to remove unreacted dopamine. When not used immediately, PdNPs are resuspended in water, and their optical absorption spectra characterized before they are flash frozen with liquid N₂ for long-term storage at -20 °C freezer. The concentration of the nanoparticle solution was determined using the solution absorbance at 808 nm ($7.3 \times 10^8 \text{ m}^{-1}\text{cm}^{-1}$).^[27,62]

Surface Modification: For surface functionalization of PdNP, 0.5 mM of the antimicrobial peptide, CWR11 (pre-incubated with 5× TCEP for 30 min at room temperature) was mixed with PdNP (5 nm) in Bicine buffer pH 8.5 (10 mM) with KCl (100 mM) and allowed to react overnight. CWR11-functionalized PdNP (PdNP-CWR11) was harvested by centrifugation at 15 000 g for 30 min. The precipitate was washed 3× with ultrapure water before being resuspended in BBS buffer for characterization and storage. The supernatant was collected to determine the concentration of the remaining unbound peptide using optical absorption spectroscopy (Section S1, Supporting Information).

Characterization: The size of the growing nanoparticles was monitored using DLS (NanoBrook Omni, Brookhaven Instruments). The surface zeta potential of the nanoparticles was determined using PALS (NanoBrook Omni, Brookhaven Instruments). The optical absorption spectra of the brownish solution of the nanoparticles were measured using a UV-vis spectrometer (Cary 60 UV-Vis, Agilent Technologies). Dried samples of the nanoparticles were further characterized using a Fourier transform infrared spectrometer (Bruker Alpha-P FTIR). To visualize the nanoparticles, both TEM (Hitachi H7500) and AFM (Nanowizard 4, JPK Instruments) were used. In TEM imaging, freshly UV-O₃-treated copper grid was placed on top of a drop of aqueous solution of PdNP, and further incubated for 5 min before drying and imaging. In AFM, a drop of aqueous solution of PdNP was allowed to dry on a glass substrate and then washed to remove loosely bound particles. Enough Milli-Q water was added on the substrate to make sure the AFM imaging was done under liquid conditions. TEM images were analyzed using the Image J software while AFM images were via the JPK Image Processing software.^[63] For the photothermal characterization of PdNP solution, a 400 mW CW 808 nm laser with diameter ≈3 mm (MDL-III-808, CNI Laser, China) was used to irradiate aqueous solutions of PdNP. A thermal imager (Compact Spot Finder IR camera Xi 80, Optris, Germany) was used to determine the solution temperature during laser irradiation.

Mechanical Characterization: To determine the mechanism of biocidal activities of PdNP and PdNP-CWR11 on *E. coli*, nanomechanical characterization was done using AFM (Nanowizard 4, JPK Instruments). Here, untreated and treated (with peptide and/or laser) bacteria were immobilized on PEI-coated polycarbonate (PC) membranes. The quantitative imaging (QI) modality of AFM was used to directly correlate structural information with mechanical properties. SNL cantilevers (Bruker), with nominal spring constants (0.28–0.35 N m⁻¹) was used. To calibrate the cantilevers, the sensitivity of the cantilever was measured by acquiring a force–distance curve on a pre-cleaned glass slide, and the spring constant was determined by thermal noise method in air.^[64] Unless otherwise stated, the following parameters were used in QI: 1 nN relative force setpoint, z-range of 500–2000 nm, cantilever speed of 83 μm s⁻¹. Analysis of AFM topography and elasticity data was done using JPK Image Processing software along with a software developed in our lab, to select and extract the Young's modulus of *E. coli*.^[65] See Section S4, Supporting Information, for more details.

Hemolytic Activity: The hemolytic activity of CWR11, PdNP, and PdNP-CWR11 was evaluated following a previously established protocol.^[66] Briefly, human red blood cells (RBC) from two separate donors (Innovative Research, Inc., USA) were washed with PBS (3×) and collected via centrifugation at 10 000 g for 10 min. 100 μL of washed RBC (in PBS) was then added to 400 μL of: i) Milli-Q H₂O (positive control), ii) PBS (negative control), and iii) increasing concentrations of CWR11,

PdNP, and PdNP-CWR11 (i.e., 0.1, 0.5, 1, 2, and 3× the MIC of each sample). The samples were kept under static conditions for 2 h at room temperature. After the 2-h incubation, the samples were then centrifuged for 3 min at 10 000 g and 100 μL of the supernatant was transferred to a 96-well plate. The absorbance at 570 and 655 nm (as a reference) was then obtained using a microplate reader (BioTek Instruments Inc., USA). The absorbance values were then used to calculate the hemolytic activity using the following:

$$\% \text{ Hemolysis} = \frac{(\text{Sample} - \text{Negative})}{(\text{Positive} - \text{Negative})} \times 100 \quad (1)$$

Photothermal Treatment: Tetracycline-resistant *E. coli* strains were grown until stationary phase (15–16 h) in LB broth containing 16 μg mL⁻¹ of the antibiotic. Cells were then harvested by centrifugation, and then washed 3× with PBS. The pelleted bacteria were then resuspended in BBS buffer. Liquid suspensions of *E. coli* with O.D. = 0.01 were mixed with different concentrations of PdNP and PdNP-CWR11, 0–2 nM. 200 mL of these solutions were then treated with 400 mW CW 808 nm laser with diameter ≈3 mm for 20 min. After laser treatment, a serial dilution of the PT-treated solution was made and plated onto LB agar plates with tetracycline (spread plate assay). The bacteria are then allowed to grow for at least 24 h at 37 °C. The number of colony forming units was determined using ImageJ image analysis software.

Fluorescence Microscopy: The antimicrobial peptide (CWR11) used in this study is a membrane destabilizing peptide. Aside from nanomechanical characterizations, its membrane activity was monitored using fluorescence microscopy: *E. coli* stained with SYTO9 and propidium iodide, PI (Live/Dead Bacterial Viability Kit, Molecular Probes). After incubating *E. coli* with the antimicrobial agent and/or laser treatment, the SYTO9:PI mixture (1:1) was added to the *E. coli* solution (1 in 1000 dilution) and incubated in the dark for 10 min. The bacterial suspension was then filtered (vacuum filtration) through a PEI-coated polycarbonate membrane (0.6 μm). Using an upright laser scanning confocal microscope (Zeiss LSM510 META) with a 100× water immersion objective, fluorescence images of *E. coli* cells were obtained, for both SYTO9 and PI fluorescence.

Supporting Information

Supporting Information is available from the Wiley Online Library or from the author.

Acknowledgements

The authors thank Prof. Regine Hengge's laboratory of Institut für Biologie/Mikrobiologie, Humboldt-Universität zu Berlin for providing them with *E. coli* strains used in this work as well as the Bloemberg Laboratory at Leiden University, The Netherlands for providing the plasmid (pMP7604). The authors also thank Dr. Bruno Chue and Dr. Durga Acharya for assistance in using the facility at the Centre for the Neurobiology of Stress (CNS) at the University of Toronto Scarborough. This work was supported by the Canada Foundation for Innovation (Project # 36544); Ontario Ministry of Research, Innovation and Science (Project # 36544); Natural Science and Engineering Research Council Canada (RGPIN-2017-06522); Connaught Fund; XSeed University of Toronto; and University of Toronto Scarborough's Research Competitiveness Fund. C.T.K. is a Feodor Lynen research fellow of the Alexander von Humboldt Foundation.

Conflict of Interest

The authors declare no conflict of interest.

Keywords

antimicrobial peptides, atomic force microscopy, localized nano-heating, photothermal treatment, polydopamine nanoparticles

Received: May 25, 2020

Revised: July 2, 2020

Published online:

- [1] G. Bloom, G. B. Merrett, A. Wilkinson, V. Lin, S. Paulin, *BMJ Glob. Health* **2017**, *2*, e000518.
- [2] C. L. Ventola, *Pharm. Ther.* **2015**, *40*, 277.
- [3] V. Hrvatin, *Can. Med. Assoc. J.* **2017**, *189*, E1199.
- [4] B. D. Brooks, A. E. Brooks, *Adv. Drug Delivery Rev.* **2014**, *78*, 14.
- [5] A. J. Huh, Y. J. Kwon, *J. Controlled Release* **2011**, *156*, 128.
- [6] E. F. Haney, S. C. Mansour, R. E. W. Hancock, *Antimicrobial Peptides: An Introduction in Antimicrobial Peptides. Methods in Molecular Biology*, Vol. 1548 (Ed: P. R. Hansen), Humana Press, New York, NY, USA **2017**, Ch. 1.
- [7] B. P. Lazzaro, M. Zasloff, J. Rolff, *Science* **2020**, *368*, eaau5480.
- [8] L. J. Zhang, R. L. Gallo, *Curr. Biol.* **2016**, *26*, R14.
- [9] M. Scocchi, M. Mardirossian, G. Runti, M. Benincasa, *Curr. Top. Med. Chem.* **2015**, *16*, 76.
- [10] C. D. Fjell, J. A. Hiss, R. E. W. Hancock, G. Schneider, *Nat. Rev. Drug Discovery* **2012**, *11*, 37.
- [11] D. I. Andersson, D. Hughes, J. Z. Kubicek-Sutherland, *Drug Resist. Updates* **2016**, *26*, 43.
- [12] J. Lei, L. C. Sun, S. Huang, C. Zhu, P. Li, J. He, V. Mackey, D. H. Coy, Q. Y. He, *Am. J. Transl. Res.* **2019**, *11*, 3919.
- [13] X. Zhu, A. F. Radovic-Moreno, J. Wu, R. Langer, J. Shi, *Nano Today* **2014**, *9*, 478.
- [14] A. Gupta, S. Mumtaz, C. H. Li, I. Hussain, V. M. Rotello, *Chem. Soc. Rev.* **2019**, *48*, 415.
- [15] P. T. Wong, S. K. Choi, *Chem. Rev.* **2015**, *115*, 3388.
- [16] M. B. Cortie, D. L. Cortie, V. Timchenko, *Int. J. Hyperther.* **2018**, *34*, 157.
- [17] P. Yuan, X. Ding, Y. Y. Yang, Q.-H. Xu, *Adv. Healthcare Mater.* **2018**, *7*, 1701392.
- [18] M. Kim, J. H. Lee, J. M. Nam, *Adv. Sci.* **2019**, *6*, 1900471.
- [19] Y. Feng, L. Liu, J. Zhang, H. Aslan, M. Dong, *J. Mater. Chem. B* **2017**, *5*, 8631.
- [20] D. G. Meeker, S. V. Jenkins, E. K. Miller, K. E. Beenken, A. J. Loughran, A. Powless, T. J. Muldoon, E. I. Galanzha, V. P. Zharov, M. S. Smeltzer, J. Chen, *ACS Infect. Dis.* **2016**, *2*, 241.
- [21] V. P. Zharov, K. E. Mercer, E. N. Galitovskaya, M. S. Smeltzer, *Biophys. J.* **2006**, *90*, 619.
- [22] R. Sean Norman, J. W. Stone, A. Gole, C. J. Murphy, T. L. Sabo-Attwood, *Nano Lett.* **2008**, *8*, 302.
- [23] L. Mocan, F. A. Tabaran, T. Mocan, T. Pop, O. Mosteanu, L. Agoston-Coldea, C. T. Matea, D. Gonciar, C. Zdrehus, C. Iancu, *Int. J. Nanomed.* **2017**, *12*, 2255.
- [24] M. A. MacKey, M. R. K. Ali, L. A. Austin, R. D. Near, M. A. El-Sayed, *J. Phys. Chem. B* **2014**, *118*, 1319.
- [25] P. Makvandi, C. Yu Wang, E. N. Zare, A. Borzacchiello, L. Na Niu, F. R. Tay, *Adv. Funct. Mater.* **2020**, *30*, 1910021.
- [26] A. M. Alkilany, C. J. Murphy, *J. Nanopart. Res.* **2010**, *12*, 2313.
- [27] Y. Liu, K. Ai, J. Liu, M. Deng, Y. He, L. Lu, *Adv. Mater.* **2013**, *25*, 1353.
- [28] J. H. Ryu, P. B. Messersmith, H. Lee, *ACS Appl. Mater. Interfaces* **2018**, *10*, 7523.
- [29] R. Mrowczynski, *ACS Appl. Mater. Interfaces* **2018**, *10*, 7541.
- [30] T. S. Sileika, H. Do Kim, P. Maniak, P. B. Messersmith, *ACS Appl. Mater. Interfaces* **2011**, *3*, 4602.
- [31] W. Lei, K. Ren, T. Chen, X. Chen, B. Li, H. Chang, J. Ji, *Adv. Mater. Interfaces* **2016**, *3*, 1600767.
- [32] C. Y. Liu, C. J. Huang, *Langmuir* **2016**, *32*, 5019.
- [33] L. Su, Y. Yu, Y. Zhao, F. Liang, X. Zhang, *Sci. Rep.* **2016**, *6*, 24420.
- [34] D. Jaque, L. Martínez Maestro, B. Del Rosal, P. Haro-Gonzalez, A. Benayas, J. L. Plaza, E. Martín Rodríguez, J. García Solé, *Nanoscale* **2014**, *6*, 9494.
- [35] D. Hu, L. Zou, B. Li, M. Hu, W. Ye, J. Ji, *ACS Biomater. Sci. Eng.* **2019**, *5*, 5169.
- [36] X. L. Fan, H. Y. Li, W. Y. Ye, M. Q. Zhao, D. ni Huang, Y. Fang, B. Q. Zhou, K. F. Ren, J. Ji, G. S. Fu, *Colloids Surf., B* **2019**, *183*, 110423.
- [37] P. C. Ray, S. A. Khan, A. K. Singh, D. Senapati, Z. Fan, *Chem. Soc. Rev.* **2012**, *41*, 3193.
- [38] D. Amin, C. Sugnaux, K. Lau, P. Messersmith, *Biomimetics* **2017**, *2*, 17.
- [39] V. Ball, *Colloids Surf. A* **2010**, *363*, 92.
- [40] K. Lim, R. R. Y. Chua, R. Saravanan, A. Basu, B. Mishra, P. A. Tambyah, B. Ho, S. S. J. Leong, *ACS Appl. Mater. Interfaces* **2013**, *5*, 6412.
- [41] K. Y. Ju, Y. Lee, S. Lee, S. B. Park, J. K. Lee, *Biomacromolecules* **2011**, *12*, 625.
- [42] R. Batul, T. Tamanna, A. Khaliq, A. Yu, *Biomater. Sci.* **2017**, *5*, 1204.
- [43] D. O. Serra, A. M. Richter, R. Hengge, *J. Bacteriol.* **2013**, *195*, 5540.
- [44] R. J. W. Lambert, J. Pearson, *J. Appl. Microbiol.* **2000**, *88*, 784.
- [45] K. A. Dill, K. Ghosh, J. D. Schmit, *Proc. Natl. Acad. Sci. U. S. A.* **2011**, *108*, 17876.
- [46] P. Leuenberger, S. Gansch, A. Kahraman, V. Cappelletti, P. J. Boersema, C. Von Mering, M. Claassen, P. Picotti, *Science* **2017**, *355*, eaai7825.
- [47] G. E. Fantner, R. J. Barbero, D. S. Gray, A. M. Belcher, *Nat. Nanotechnol.* **2010**, *5*, 280.
- [48] M. Meincken, D. L. Holroyd, M. Rautenbach, *Antimicrob. Agents Chemother.* **2005**, *49*, 4085.
- [49] E. R. Rojas, G. Billings, P. D. Odermatt, G. K. Auer, L. Zhu, A. Miguel, F. Chang, *Nature* **2018**, *559*, 617.
- [50] D. Alsteens, D. J. Müller, Y. F. Dufrêne, *Acc. Chem. Res.* **2017**, *50*, 924.
- [51] S. V. Bhat, T. Sultana, A. Körnig, S. McGrath, Z. Shahina, T. E. S. Dahms, *Sci. Rep.* **2018**, *8*, 8305.
- [52] W. Qiang, W. Li, X. Li, X. Chen, D. Xu, *Chem. Sci.* **2014**, *5*, 3018.
- [53] M. Bagheri, M. Beyermann, M. Dathe, *Antimicrob. Agents Chemother.* **2009**, *53*, 1132.
- [54] G. Gao, K. Yu, J. Kindrachuk, D. E. Brooks, R. E. W. Hancock, J. N. Kizhakkedathu, *Biomacromolecules* **2011**, *12*, 3715.
- [55] L. C. Shriver-Lake, G. P. Anderson, C. R. Taitt, *Langmuir* **2017**, *33*, 2878.
- [56] T. J. Silhavy, Jd. Kahne, S. Walker, *Cold Spring Harbor Perspect. Biol.* **2010**, *2*, a000414.
- [57] W. Jo, M. J. Kim, *Nanotechnology* **2013**, *24*, 195104.
- [58] R. Batul, M. Bhave, P. J. Mahon, A. Yu, *Molecules* **2020**, *25*, 2090.
- [59] J. Song, H. Liu, M. Lei, H. Tan, Z. Chen, A. Antoshin, G. F. Payne, X. Qu, C. Liu, *ACS Appl. Mater. Interfaces* **2020**, *12*, 8915.
- [60] D. Park, J. Kim, Y. M. Lee, J. Park, W. J. Kim, *Adv. Healthcare Mater.* **2016**, *5*, 2019.
- [61] D. Liu, L. Ma, L. Liu, L. Wang, Y. Liu, Q. Jia, Q. Guo, G. Zhang, J. Zhou, *ACS Appl. Mater. Interfaces* **2016**, *8*, 24455.
- [62] B. Poinard, S. Z. Y. Neo, E. L. L. Yeo, H. P. S. Heng, K. G. Neoh, J. C. Y. Kah, *ACS Appl. Mater. Interfaces* **2018**, *10*, 21125.
- [63] C. A. Schneider, W. S. Rasband, K. W. Eliceiri, *Nat. Methods* **2012**, *9*, 671.
- [64] J. L. Hutter, J. Bechhoefer, *Rev. Sci. Instrum.* **1993**, *64*, 1868.
- [65] C. T. Kreis, R. M. A. Sullan, *Nanoscale* **2020**, <https://doi.org/10.1039/D0NR03646C>.
- [66] Y. S. Lin, C. L. Haynes, *J. Am. Chem. Soc.* **2010**, *132*, 4834.